Mol Neurobiol
DOI 10.1007/s12035-014-9082-1

Neuroglobin Expression in the Mammalian Auditory System

Stefan Reuss · Ovidiu Banica · Mirra Elgurt · Stephanie Mitz · Ursula Disque-Kaiser · Randolf Riemann · Marco Hill · Dawn V. Jaquish · Fred J. Koehrn · Thorsten Burmester · Thomas Hankeln · Nigel K. Woolf

Received: 23 September 2014 / Accepted: 29 December 2014

Abstract The energy-yielding pathways that provide the large amounts of metabolic energy required by inner ear sensorineural cells are poorly understood. Neuroglobin (Ngb) is a neuron-specific hemoprotein of the globin family, which is suggested to be involved in oxidative energy metabolism. Here, we present quantitative real-time reverse transcription PCR, in situ hybridization, immunohistochemical, and Western blot evidence that neuroglobin is highly expressed in the mouse and rat cochlea. For primary cochlea neurons, Ngb expression is limited to the subpopulation of type I spiral ganglion cells, those which innervate inner hair cells, while the subpopulation of type II spiral ganglion cells which innervate the outer hair cells do not express Ngb. We further investigated Ngb distribution in rat, mouse, and human auditory brainstem centers, and found that the cochlear nuclei and superior olivary complex (SOC) also express considerable amounts of Ngb. Notably, the majority of olivocochlear neurons, those which provide efferent innervation of outer hair cells as identified by neuronal tract tracing, were Ngb-immunoreactive. We also observed that neuroglobin in the SOC frequently co-localized with neuronal nitric oxide synthase, the enzyme responsible for nitric oxide production. Our findings suggest that neuroglobin is well positioned to play an important physiologic role in the oxygen homeostasis of the peripheral and central auditory nervous system, and provides the first evidence that Ngb signal differentiates the central projections of the inner and outer hair cells.

Keywords Neuroglobin · Cochlea · Hair cell · Spiral ganglion · Mice · Hearing · Auditory

Abbreviations

pb	Base pairs
DPO	Dorsal paraolivary nucleus
FG	Fluoro-Gold
GAPDH	Glyceraldehyde-3-phosphate dehydrogenase

Electronic supplementary material The online version of this article (doi:10.1007/s12035-014-9082-1) contains supplementary material, which is available to authorized users.

S. Reuss (✉)
Department of Nuclear Medicine, University Medical Center, Johannes Gutenberg-University, Langenbeckstr. 1, Bld. 210, 55101 Mainz, Germany
e-mail: reuss@uni-mainz.de

O. Banica · M. Elgurt · S. Mitz
Department of Anatomy and Cell Biology, University Medical Center, Johannes Gutenberg-University, 55099 Mainz, Germany

U. Disque-Kaiser
Department of Radiation Oncology, University Medical Center, Johannes Gutenberg-University, 55101 Mainz, Germany

R. Riemann
Department of ENT, Elbe-Kliniken, 21682 Stade, Germany

M. Hill · T. Hankeln
Institute of Molecular Genetics, Johannes Gutenberg-University, 55099 Mainz, Germany

D. V. Jaquish · F. J. Koehrn · N. K. Woolf
Department of Surgery, University of California at San Diego, San Diego, CA 92093-0604, USA

D. V. Jaquish · F. J. Koehrn · N. K. Woolf
Veterans Affairs Research Service, VA San Diego Healthcare System, San Diego, CA 92093-0604, USA

T. Burmester
Institute of Zoology and Zoological Museum, University of Hamburg, Hamburg, Germany

Published online: 31 January 2015

IHC	Inner hair cells
ISH	In situ hybridization
LOC/MOC	Lateral/medial olivocochlear neurons
LSO	Lateral superior olive
MNTB	Medial nucleus of the trapezoid body
MSO	Medial superior olive
Ngb	Neuroglobin
nNOS	Neuronal nitric oxide synthase
NO	Nitric oxide
OHC	Outer hair cells
OCN	Olivocochlear neurons
PBS	Phosphate-buffered 0.9 % saline
RPO	Rostral paraolivary nucleus
rt-RT-PCR	Real-time reverse transcription polymerase chain-reaction
RT	Room temperature
Sgn	Spiral ganglion neurons
SOC	Superior olivary complex
SPO	Superior paraolivary nucleus
VNTB	Ventral nucleus of the trapezoid body
VPO	Ventral paraolivary nucleus

Introduction

The globin family is comprised of small porphyrin-containing proteins, which can reversibly bind O_2 by means of an iron (Fe^{2+}) ion of the heme prosthetic group [1, 2]. Besides the better known examples of hemoglobin (Hb) and myoglobin (Mb), the vertebrate globin family includes six additional members: neuroglobin (Ngb) [3], cytoglobin (Cygb) [4–6], globin E (GbE) [7], globin X (GbX) [8], globin Y (GbY) [9], and androglobin (Adgb) [10]. The vertebrate globins have a complex evolutionary history and may serve different functions which are, however, often only poorly defined [11]. While Hb, Mb, Ngb, Cygb, and Adgb are present in most jawed vertebrates [10, 12], GbE, GbX, and GbY appear to have been lost in placental mammals and other vertebrate taxa [11].

Ngb has been identified in a wide range of vertebrates, and its structure has been highly conserved (e.g., there is 94 % amino acid sequence identity between human and murine Ngb) [13]. Ngb is mainly expressed in neurons of the central and peripheral nervous systems and in endocrine tissues [3, 14–24]. Ngb has also been found in the retinae of man, mouse, and guinea pig [25–28]. Within the retina, Ngb is expressed primarily at sites of high oxygen consumption: the inner segments of photoreceptor cells, the inner and outer nuclear layers, and the retinal ganglion cell layer [25, 26]. There is convincing evidence that in retina and brain Ngb is associated with mitochondria and thus with oxidative metabolism [25, 26, 18]. Moreover, across vertebrates total Ngb levels in brain seem to be positively correlated with species' tolerance for hypoxia [29, 24, 20].

Experimental investigations have demonstrated that Ngb serves to protect cultured cerebral neurons from hypoxia in vitro [30]. Ngb may also help the brain in vivo to resist neuronal injury during experimental stroke [31], although studies with knockout mice rather contradict this conclusion [32]. In summary, while the exact physiological role of Ngb is still a matter of debate [33, 34], it is likely that Ngb contributes to local O_2 supply or, alternatively, provides protection from reactive oxygen species (ROS).

The anatomical structure of the mammalian inner ear makes the neurosensory hair cells and vestibulocochlear nerve neurons uniquely vulnerable to hypoxia/ischemia [35]. Although the anatomy of the cochlea has been well described and considerable progress has been made in characterizing the structural and physiological properties of the inner ear (cf. [36–40], at present, we still know relatively little about the specific cellular mechanisms by which the inner ear satisfies its normal metabolic energy demands and defends itself against pathologic conditions. Early studies of oxygen consumption in the cochlea have suggested that metabolic rates were higher in external wall structures (e.g., stria vascularis) than in sensorineural cells (reviewed in [41]). Subsequent investigations utilizing the 2-deoxyglucose (2-DG) radiotracer technique determined that acoustic stimulation alters cochlear metabolism: in silence the rate of 2-DG incorporation in the cochlea was highest in external wall structures (i.e., stria vascularis, spiral ligament, and spiral prominence), and relatively low in neurosensory cells (i.e., inner and outer hair cells, and vestibulocochlear (VIIIth cranial) nerve ganglia), while noise exposure significantly increased the rate of 2-DG uptake in the same cochlear external wall structures and auditory neurosensory cells [42–44].

The metabolic energy required for neurosensory cell function in the cochlea is provided primarily by adenosine triphosphate (ATP). ATP levels have been measured in cultured cochlear hair cells [41] and CNS neurons [45], and these levels were found to be on the same order of magnitude as freeze-dried outer hair cell preparations [46]. In addition, it has been demonstrated that the induction of cochlear pathology (e.g., hypoxia/ischemia) significantly reduces the ATP content of the organ of Corti in vivo [47]. However, questions remain about the relative contributions of the glycolytic and oxidative pathways to the synthesis and maintenance of ATP levels in the inner ear. Glycolysis results in the formation of lactate, but since attempts to measure lactate in the cochlea have failed [48], it has long been assumed that low-level aerobic metabolism is the primary source of cochlear ATP. On the other hand, there is evidence that outer hair cells deprived of glucose ex vivo generate ATP, which suggests that these sensory cells may also possess unidentified intracellular metabolic

substrates that can augment oxidative phosphorylation under hypoxic conditions [41].

Oxygen required for aerobic glucose metabolism is supplied to the inner ear by the Hb of the blood. While the spiral (auditory) and Scarpa's (vestibular) ganglia of the vestibulocochlear nerve are well vascularized by radiating capillary arcades, the neuroepithelia of the auditory (i.e., organ of Corti), and vestibular (i.e., maculae of the utricle and saccule, and cristae ampullares of the semicircular canals) systems do not receive any direct blood supply [49]. Consequently, oxygen must diffuse relatively large distances to reach the auditory and vestibular sensory hair cells. Notably, the vascular anatomy of the inner ear is homologous to that of the eye, since the retina similarly lacks any direct blood supply to its sensory cells (i.e., photoreceptors) [50]. Because the inner ear and eye share similar challenges in providing an adequate supply of oxygen to their neurosensory cells during periods of oxidative stress, we hypothesized that the auditory and vestibular systems may have evolved similar cellular mechanisms to fuel their oxidative metabolic demands as those present in the retina.

Besides one report that Ngb is expressed by spiral ganglion neurons [51], detailed information about the distribution of Ngb in mammalian peripheral and central auditory system is lacking. We, therefore, studied the cochlea of rats and mice, and the auditory brainstem of rats, mice, and man, using Ngb immunohistochemistry, in situ hybridization, Western blotting, quantitative rt-RT-PCR, and neuronal tract tracing to characterize Ngb-expressing anatomical regions and neuronal cell types. We describe here that Ngb is highly expressed in a subpopulation of primary afferent neurons in the vestibulocochlear nerve but not in auditory sensory hair cells. Ngb is also present in the auditory brainstem, in particular in the superior olivary complex, and in a functionally important subpopulation, the olivocochlear neurons.

Materials and Methods

Animals

The experiments were conducted on (1) 6–10-week-old-male C.B-17 mice (Taconic Farms, Germantown, NY, USA) housed under constant conditions (light:dark 12:12 h, temperature 22+2 °C) with food and water ad libitum at the VA San Diego Healthcare System (VASDHS) Veterinary Medical Unit. Experimental protocols were approved by the VASDHS Institutional Animal Care and Use Committee, and conformed to the PHS "Guide for the Care and Use of Laboratory Animals," (2) male Balb/C-mice, aged 2 months, and (3) 9–12-week-old-male Sprague-Dawley rats, held under constant conditions (see group 1) in the animal facility unit of the Department of Anatomy and Cell Biology, Johannes Gutenberg-University, Mainz, Germany. Animals of groups 2 and 3 were bred in-house. Experimental protocols (animal housing and neuronal tracing) were approved by the local Administration District Official Committee and were in accordance with the published European Health Guidelines. All efforts were made to minimize the number of animals and their suffering.

Neuroglobin Immunohistochemistry

Mouse cochleae and brains were dissected from animals of the C.B-17 strain that were killed by cervical dislocation. The cochleae were then immersion-fixed in 5 % paraformaldehyde in phosphate-buffered 0.9 % saline (PBS) for 2 h at 4 °C, and then decalcified in 10 % EDTA at 4 °C. Decalcified cochleae were subsequently immersed in 30 % sucrose until they sank, embedded in OCT, frozen, sectioned at 10 μm, collected onto BioBond-coated (Ted Pella, Redding, CA). Fisher SuperFrost slides (Fisher Scientific, Tustin, CA), air and vacuum dried, and then stored until needed at −70 °C. Two different Ngb antibodies directed against a synthetic peptide which covers the conserved amino acid positions 55–70 of mammalian Ngb (H2N-CLSSPEFLDHIRKVML-CONH2) [30, 25] were independently raised in rabbits. One was produced by Strategic Biosolutions Inc. (San Diego, CA), the other was produced by Eurogentec (Köln, Germany, see [25]). Antibodies were affinity-purified using a SulfoLink kit (Pierce Biochemicals, Rockford, IL) as described by the manufacturer.

Mouse sections on glass slides were washed in PBS-0.1 % Triton X-100, treated with blocking solution (10 % normal donkey serum+5 % BSA in PBS-0.1 % Triton X-100), incubated overnight at RT with Ngb antibody (1:200; Strategic Biosolutions) and mouse monoclonal anti-peripherin intermediate filament protein antibody (1:25; Chemicon, Temecula, CA) diluted in blocking solution (Mouse-On-Mouse PK-2200 Kit, Vector Laboratories, Burlingame, CA) overnight at 4 °C. Slides were washed and incubated with secondary donkey anti-rabbit antibody conjugated to Alexa 594 (1:300) and donkey anti-mouse antibody conjugated to Alexa 488 (1:300; Molecular Probes, Eugene, OR) in PBS for 1 h in the dark. Slides were washed and stained with bisbenzimide (nuclear stain, Sigma, St. Louis, MO), washed again, and coverslipped with Prolong Mounting Media (Molecular Probes, Eugene, OR). Negative control experiments which substituted normal rabbit and mouse IgG for the primary antibodies resulted in the complete absence of staining.

Rats were killed by ether overdose at the middle of the light period and immediately perfused transcardially with PBS to which 15,000 IU heparin/L were added, at RT, followed by an ice-cold paraformaldehyde-lysine-periodate solution (PLP; [52]. The right atrium was opened to enable venous outflow. Cochleae were decalcified as described above, sectioned at 30-μm thickness and mounted on gelatinized glass slides.

Sections were then incubated overnight at RT with Ngb antibody (1:500; Eurogentec), to which 1 % normal donkey serum and 0.1 % Triton-X 100 were added. After three rinses in PBS, the reaction was visualized using Cy3 conjugated to an $F(ab)_2$ fragment of a donkey anti-rabbit IgG (1:200 in PBS; Jackson Immuno-Research, West Grove, PA). Sections were dried, cleared in xylene, and covered.

For brainstem immunohistochemistry, PLP-perfused rat and mouse brains were removed, postfixed in PLP for 1 h, and stored overnight at 4 °C in phosphate-buffered 30 % sucrose for cryoprotection. They were then sectioned serially at 40-μm thickness on a freezing microtome in the frontal plane. Sections were collected in PBS and, for immunohistochemistry, incubated free-floating overnight at RT in Ngb antibody (1:500, Eurogentec), and processed further as described above for the rat cochlea.

RNA Extraction

Total RNA was extracted from frozen C.B-17 mouse whole brains and cochleae using TRizol reagent (Invitrogen, Carlsbad, CA), and from Balb/C mouse whole brains using the RNeasy kit (Qiagen, Hilden, Germany), and subsequently treated with DNase I Amplification Grade (Invitrogen) according to the manufacturer's protocols.

DNA Synthesis and Cloning of Ngb-cDNA for ISH

Ngb cDNA was generated using the SuperScript One-Step RT-PCR with Platinum Taq (Invitrogen) according to the manufacturer's protocol. In brief, 500 ng of DNase I-treated total RNA was added to 1× reaction mix buffer (containing 0.2 mM of each dNTP and 1.2 mM $MgSO_4$), 1 μl RT/Platinum Taq Mix and 0.2 μM of sense and antisense Ngb primers: sense primer 5′-GTTGACTGCACCCACGCCT-3′; antisense primer 5′-GCACCACAGCTCCGTAGAGT-3′ (GenBank accession number NM-022414), with the total volume being 50 μl. The reaction was then given into a Deltacycler II (Ericomp Inc., San Diego, CA) and cycled at 50 °C for 30 min then at 94 °C for 2 min, followed by 40 cycles of 94 °C for 30 s, 65 °C for 30 s, and 72 °C for 1 min, with a final annealing extension at 72 °C for 5 min. A 487 bp Ngb fragment was generated and then cloned using the TOPO Dual Vector Cloning System (Invitrogen). The fragment was then sequenced by the UCSD/VMRF CFAR Genomics Core Facility for verification.

Neuroglobin In Situ Hybridization

For the detection of Ngb-mRNA in the mouse cochlea, the 487 bp Ngb cDNA was cut with EcoRV and PstI to generate a 308 bp fragment (290 bp of it being Ngb) which was then subcloned into the EcoRV, PstI sites of the pSP72 vector (Promega, Madison, WI). Sense and antisense Ngb probes were generated by linearizing the subclone with HindIII or EcoRV, respectively, followed by labeling using the DIG RNA labeling kit (Roche, Indianapolis, IN) according to the manufacturer's protocol. Paraffin-embedded sections were deparaffinized in CitriSolve (Fisher Scientific, Waltham, MA), hydrated in graded alcohols, and rinsed 2× in 1×PBS for 5 min prior to prehybridization. For prehybridization, the sections were placed in 0.2 N HCl at RT for 20 min, dipped in dH_2O, put in 2× standard saline citrate (SSC) at 70 °C for 30 min, dipped in dH_2O, digested in 20 mM Tris pH 7.4, 2 mM $CaCl_2$+4 μg/ml proteinase K at 37 °C for 30 min, and digestion terminated with 0.2 % glycine in 1×PBS for 30 s, followed by 2× 5-min washes in 1×PBS, 3 min in 0.1 M triethanolamine (TEA) pH 8.0, followed by an acetylation step of 1:400 acetic anhydride in TEA for 10 min. Slides were then passed 2× in 2× SSC for 2 min, dehydrated in graded alcohols, and air-dried.

The hybridization buffer contained 50 % deionized formamide, 10 % dextran sulfate, 0.3 M NaCl, 10 mM Tris pH 7.6, 5 mM EDTA pH 7.6, 1X Denhardt's solution, 100 μg/ml yeast tRNA and 250 μg/ml sheared herring sperm DNA. Hybridization was conducted overnight at 42 °C with 0.5 μg/μl of probe per slide. Washes consisted of 2× 15 min in 2×SSC+0.1 % Triton X-100 at 42 °C, 15 min in 0.2×SSC+0.1 % Triton X-100 at 42 °C, 15 min in 0.1×SSC+0.1 % Triton X-100 at 42 °C, and 2× 15 min in 1× washing buffer (100 mM Tris+150 mM NaCl pH 7.5)+0.5 % Triton X-100 at RT. Blocking was with 2 % blocking buffer (Blocking Reagent, Roche, Indianapolis, IN) in 1× washing buffer+0.5 % Triton X-100 at RT for 30 min. Slides were then incubated with a 1:400 dilution of anti-DIG antibody-AP (Roche) in 1 % blocking buffer (2 % blocking buffer diluted 1:1 with 1× washing buffer) at RT for 1.5 h. Slides were then washed 3× 5 min at RT in 1× washing buffer+0.5 % Triton X-100, followed by an equilibration in 1X detection buffer (100 mM Tris+100 mM NaCl pH 9.5+10 mM $MgCl_2$+240 μg/ml Levaminsol) at RT for 2 min. Development was carried out overnight in the dark at RT using 1X detection buffer+0.33 mg/ml NBT+0.16 mg/ml BCIP. Development was stopped by dipping the slides 2× in dH_2O for 5 min. Sections were counterstained for 1 s in hematoxylin, and slides were coverslipped with crystal mount (Biomedia Corp., Foster City, CA).

For the detection of Ngb-mRNA in the rat brainstem, PLP-perfused brains were postfixed in PLP for 1 h and stored overnight at 4 °C in phosphate-buffered 30 % sucrose for cryoprotection. They were then sectioned serially at 40-μm thickness on a freezing microtome in the frontal plane. Sections were collected in PBS, mounted on silanized glass slides and processed for in situ hybridization. The hybridization procedures used on brainstem slices were described before [15] and resembled those used on cochlea sections (see above). In

brief, digoxigenin-labeled sense (negative control) and antisense RNA probes were in vitro transcribed by SP6 RNA polymerase (DIG RNA Labeling Kit, Roche, Mannheim, Germany), using polymerase chain reaction (PCR)-generated templates covering the 453-bp mouse Ngb coding region (accession no. AJ245945). For template generation, a SP6 RNA polymerase promoter sequence was attached to the 5′ end of the sense or antisense PCR primers. For prehybridization, slices were incubated for 1 min with proteinase K (10 μg/ml) in PBS/Tween 20. Digestion was terminated with 0.2 % glycine in phosphate-buffered saline (PBS)/Tween 20 followed by 3×5 min in PBS/Tween 20 and 1×5 min in PBS. RNA probes were diluted in 2× SSC/50 % formamide and sections were incubated with the probe at 42 °C overnight. Slides were washed first in 2× SSC, followed by 0.1× SSC at 60 °C for 20 min. Preparations were then treated with a mixture of RNAse A (25 μg/ml) for 30 min at 37 °C in a wet chamber, and thereafter washed in PBS/Tween 20. After blocking for 15 min in 1 % blocking reagent (Roche) in 0.1 M Tris and 0.15 M NaCl at pH 7.5, label was detected by alkaline phosphatase-coupled anti-digoxigenin antibodies (diluted 1:100 in 1 % blocking reagent in 0.1 M Tris and 0.15 M NaCl, pH 7.5); 30-min incubation at 37 °C, washing in PBS/Tween 20 and NBT buffer (0.1 M Tris, 0.1 M NaCl, 0.05 M $MgCl_2$-hexahydrate pH 9.5), and subsequent incubation with nitro-blue-tetrazolium/5-bromo-4-chloro-3-indolyl-phosphate substrate (1:50 diluted in NBT buffer; 30–45 min 37 °C in the dark). Substrate reaction was stopped by PBS washing. Sections were dried, covered by PBS/glycerol (1:1) solution, and coverslipped.

Quantitative Real-Time Reverse-Transcription Polymerase Chain-Reaction (rt-RT-PCR)

DNase I-treated total RNA (1 μg; see "RNA Extraction") was reverse transcribed using SuperScript II RNase H-Reverse Transcriptase (Invitrogen), according to the manufacturer's protocol. Reactions were primed using oligo$(dT)_{12\text{-}18}$ primers and the total volume/reaction was 20 μl. Following completion of the reaction, samples were brought to 10 ng/μl final volume with 5 μl being used for rt-RT-PCR.

Ngb-mRNA expression in C.B-17 mouse whole brains and cochleae was measured by quantitative rt-RT-PCR, based on TaqMan method, using the ABI PRISM 7700 Sequence Detection System (Applied Biosystems, Foster City, CA). Primers and probe sequences for Ngb (GenBank accession number AJ245945) were designed using Primer Express software (Applied Biosystems): forward primer 5′-TGCTGCCT CTCTTCCAGTACAA-3′; reverse primer 5′-GGAATTCT GGAGAGGAGAGACAGT-3′; and probe 5′-CCGCCAGT TCTCCAGCCCTGAG-3′. Quantitative rt-RT-PCR reactions were performed by the UCSD/VMRF CFAR Genomics Core. The total RNA was normalized by the amount of glyceraldehyde-3-phosphate dehydrogenase (GAPDH) amplified in each reaction. A GAPDH standard curve was prepared as the endogenous reference, and an Ngb standard curve was constructed based on tenfold dilutions of the 487 bp Ngb cDNA ranging from 1 ng to 10 μg. A total of 50 ng of the RT product was used for each sample reaction, with all reactions run in duplicate. Results were obtained by using the relative standard curve analysis (Applied Biosystems User Bulletin #2). The amount of sample Ngb and GAPDH target was then determined from the appropriate standard curve. For each sample the averaged Ngb target values were divided by the averaged GAPDH target values to obtain the normalized amount of Ngb mRNA target. The standard deviation for the normalized amount of Ngb mRNA target was calculated using the following formulae:

$$\mathrm{SD} = \sqrt{\mathrm{CV}_{\mathrm{Ngb}^2} + \mathrm{CV}_{\mathrm{GAPDH}}} \tag{1}$$

where

$$\mathrm{CV} = \frac{s}{x} = \frac{\mathrm{standarddeviation}}{\mathrm{meanvalue}} \tag{2}$$

One of the brain samples (brain #1) was arbitrarily chosen as the calibrator, and the average normalized Ngb sample value was divided by the average normalized calibrator Ngb value. Thus, the calibrator (i.e., brain #1) constituted the 1× sample, and the relative amount of target Ngb mRNA in the different samples was expressed as an *n*-fold modulation difference relative to the calibrator.

For the quantification of Ngb-mRNA from specific brain regions, including the SOC and cochlear nucleus, we cut fresh mouse brains in 1-mm thick coronal slices and microdissected the regions using neuropunch needles with defined inner diameter (Fine Science Tools, Heidelberg, Germany). Samples were processed as described above, with the following modifications. For the TaqMan assay, we used the QuantiTect Probe PCR-Kit (Qiagen, Hilden, Germany) and the ABI PRISM 7000 Sequence Detection System (Applied Biosystems) with the following primers for Ngb, designed using IDTSciTools OAnalyzer 3.0 (Integrated DNA Technologies, San Diego, CA).

Forward primer 5′-GAAGCATCGGGCAGTG-3; reverse primer 5′-AGGCACCTCTCCAGCATGTAGAG-3; and probe 6-FAM-5′-CTCAGCTCCTTCTCGACAGT-3-Dark Quencher. Acidic ribosomal protein (ARP) [forward primer 5′-AGGGCGACCTGGAAGTCC-3; reverse primer 5′-GCATCTGCTTGGAGCCCA-3] was used for RNA normalization.

The SPSS 12.0 program (SPSS, München, Germany) was used for statistical analysis and to generate boxplots.

Olivocochlear Neuronal Tracing

These experiments were performed on five rats, which were anesthetized with tribromoethanol (0.3 g/kg b.w., i.p.) and received pressure-injections of 200 nl of a 5 % Fluoro-Gold solution (FG, Fluorochrome, Englewood, CO; dissolved in distilled water) into the left scala tympani via the round window. The surgical approach was described previously [53, 54]. After 5 days, rats were killed by ether overdose and perfused with PLP as described above.

Double Immunofluorescence of Brainstem Sections

PLP-perfusion-fixed brains from Balb/C-mice were cryoprotected and sectioned as described above. Sections were incubated with Ngb-antibody (1:500, Eurogentec), visualized by Cy3 and, simultaneously, with sheep anti-neuronal nitric oxide synthase (nNOS, 1:500 in PBS; Abcam, Cambridge, England), visualized by anti-sheep IgG coupled to Cy2 (1:200; Jackson, West Grove, PA), and treated further as described above. Control incubations showed that blocking the antisera with the respective antigens as well as omission of single or both primary and/or secondary antisera resulted in the absence of respective staining, and that no cross-reactivity between primary and secondary antibodies was present.

Cell Counting

From each section, FG-labeled cells of the brainstem were quantified with regard to their location within the SOC. Neurons exhibiting immunoreactivity to the antibodies tested were counted when immunoreactivity was clearly over the background level. They were manually counted from the incubated sections using an Olympus BX 51 research microscope (see "Image Analysis"). Counts were corrected according to Abercrombie [55] to prevent double counting of cells. Single- and double-labeled neurons were quantified separately and the respective percentages were calculated for each nucleus.

Brainstem regions were identified using the stereotaxic brain atlases for rat and mouse [56, 57], and the overviews given by Schwartz [58], Warr [59], Kulesza et al. [60], and Malmiera and Merchan [61]. According to Warr [59] and Vetter and Mugnaini [62], FG-labeled neurons were divided into three subgroups: lateral olivocochlear (LOC) neurons in the lateral superior olive (LSO), shell-neurons (surrounding the LSO, including periolivary regions), and medial OC (MOC) neurons in the ventral nucleus of the trapezoid body (VNTB) and rostral periolivary region (RPO).

Human Brainstem Immunohistochemistry

These studies were performed on sections from the human brainstem. Material was kindly provided by Dr. Thorsten Fink, Department of Pathology, HSK Wiesbaden, Germany. Specimens were derived from a woman who died at the age of 73 from peritonitis and septic shock, and a man died at the age of 74 ears from pneumonia. Neither one suffered from any known neurological disease. Brainstems were taken postmortem, immersion-fixed, and stored in formalin at 4 °C.

For analysis, the brainstems were cut in half at the median anterior fissure, and a section of 15-mm thickness was taken from the region cranial to the border between medulla oblongata and pons. This specimen was cryoprotected in phosphate-buffered sucrose, cut in 40-μm sections, and stored in 10 mM PBS at 4 °C.

Due to the high levels of autofluorescence found in the aged human brain specimens, and the unsatisfying results of quenching procedures, we used a non-fluorescent detection method. In brief, after incubation in primary Ngb-antibody (1:500, Eurogentec), sections were washed in PBS, incubated for 1.5 h at RT in a biotin-conjugated $F(ab)_2$ fragment of a donkey anti-rabbit IgG (1:200 in PBS; Jackson Labs, West Grove, PA), and processed for immunohistochemistry according to the avidin-biotin-peroxidase-complex method (ABC Set, Vector Labs, Burlingame, CA; [63], using alpha-naphthol as chromogen. Sections were mounted on gelatin-coated slides, dried, and coverslipped.

Image Analysis

Mouse cochlea immunohistochemistry and in situ hybridization slides were examined using a Zeiss Axioplan II microscope equipped with a KX85 CCD camera (Apogee Instruments, Tucson, AZ). Digital images were processed and optimized using either Image Pro (Media Cybernetics, Silver Springs, MD) or Adobe Photoshop (San Jose, CA). Quantification of somatic fluorescence was accomplished using only the linear range of the digital camera. Deconvolution images were collected using a DeltaVision Restoration microscope system (Applied Precision Inc., Issaquah, WA) equipped with a Sony Photometrics Coolsnap HQ charged-coupled device (CCD) camera system (10 MHz, 12 bit, 1392×1040; Sony, Burbank, CA) attached to an inverted, wide-field fluorescent Nikon TE-200 microscope (Nikon Inc., Kanagawa, Japan). Optical sections were acquired using Nikon oil immersion objectives in 0.2-μm steps in the z-axis using the attached Applied Precision Inc. motorized stage. Images were saved, processed, and analyzed on SGI workstations (Oxygen & Octane computers; Silicon Graphics, Mountain View, CA) using the DeltaVision SoftWorx software package (version 2.50).

Sections from rat cochlea, as well as from rat, mouse, and human brainstem (ISH, neuronal tracing, and double

immunofluorescence material) were analyzed using an Olympus BX51 research microscope equipped with an epifluorescence unit and filter sets for FG (excitation center wavelength 360 nm, bandwidth 50 nm), Cy2 (480/40 nm) and Cy3 (540/25 nm) as well as a digital color camera operated using the AnalySIS (Soft Imaging System, Münster, Germany) image processing program. Images were merged, and contrast and brightness adjusted using Adobe Photoshop (Adobe Systems Inc., San Francisco, CA).

Results

Experiments described here were conducted on mouse, rat, and human material.

Localization of Neuroglobin Protein

Immunohistochemical staining of rat and mouse cochlea with either rabbit-raised Ngb antibody produced strong immunostaining in the primary auditory sensory ganglia (i.e., spiral ganglion neurons, Fig. 1). While the great majority of the spiral ganglion neurons within Rosenthal's canal in each turn of the cochlea exhibited intense Ngb immunoreactivity, we consistently noted a small subpopulation of spiral ganglion neurons which displayed little or no Ngb immunostaining (Fig. 1b). Those spiral ganglion neurons which were intensely immunolabeled by the Ngb antiserum exhibited somatic characteristics (e.g., large perikarya) which have previously been associated with type I spiral ganglion neurons (SgnI; Supplementary Fig 5A) [64]. In contrast, those spiral ganglion neurons which showed little, or no Ngb immunostaining generally appeared to have the smaller perikarya associated with type II spiral ganglion neurons (SgnII; Supplementary Fig 5A) [64]. Notably, the two spiral ganglion neuronal subpopulations can be definitively distinguished based on their neurofilament immunostaining properties: anti-peripherin (56 kDa neurofilament) antibody strongly immunostains SgnII, but not SgnI neurons [65].

We therefore subjected sections from mouse cochlea for double-label immunostaining with anti-Ngb and anti-peripherin antibodies. At the qualitative level,

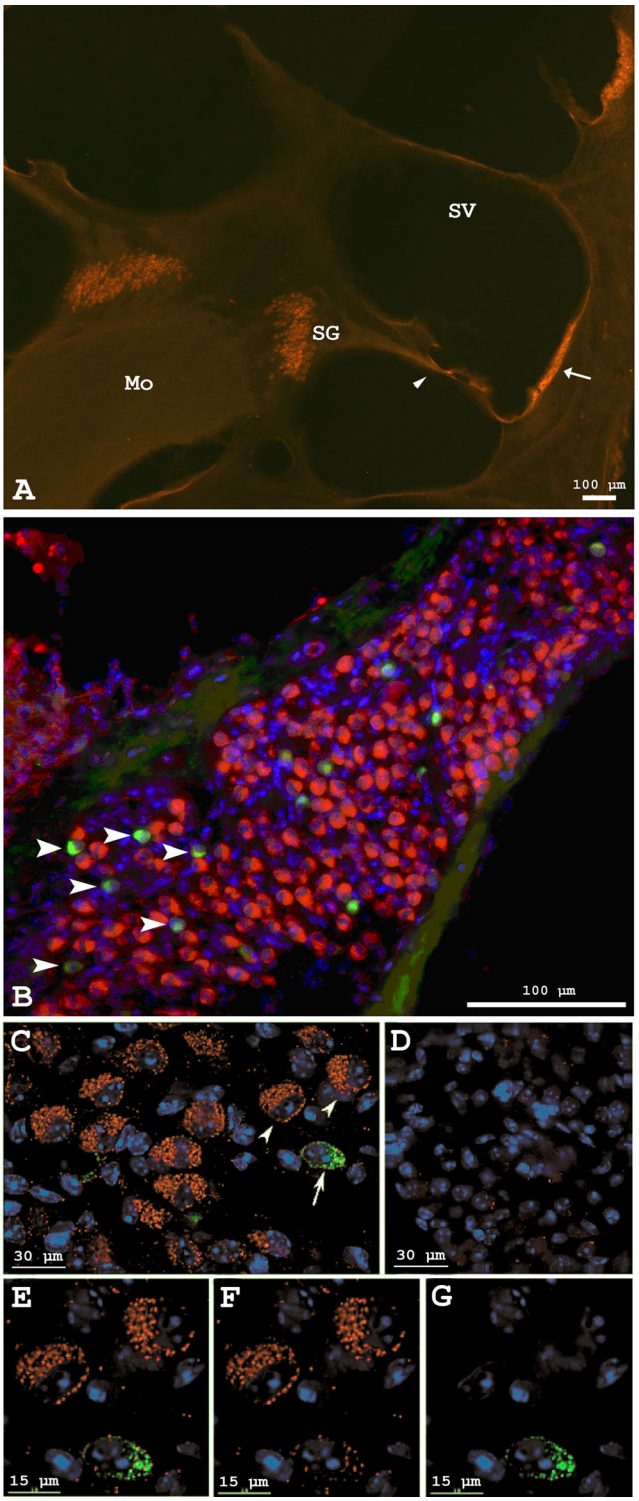

Fig. 1 Neuroglobin protein distribution in the cochlea. **a** Ngb immunofluorescence (*red*) in spiral ganglion neurons, stria vascularis (*arrow*), and basilar membrane (*arrowhead*) of the rat cochlea. *Mo* modiolus, *SV* scala vestibuli, *SG* spiral ganglion cells in Rosenthal's canal. *Scale bar*=100 µm. **b** Double-label immunostaining of mouse spiral ganglion cells with anti-Ngb (*red*) and anti-peripherin (*green*). SgnI cells were immunolabeled with anti-Ngb while SgnII cells (*arrowheads*) were immunostained with anti-peripherin. Nuclei are stained blue with bisbenzimide. **c–g** Deconvolution images illustrating differential Ngb immunostaining in SgnI and SgnII cells of the mouse cochlea. **c** Double-label immunostaining with anti-Ngb (*red*: *arrowheads*) and anti-peripherin (*green*: *arrow*). **d** Control omitting primary anti-Ngb and anti-peripherin antibodies. **e–g** High-power images of the three cells indicated by *arrows* and *arrowheads* in (**c**), **e** SgnI and SgnII (combined red and green channels), **f** SgnI only (red without green channel), and **g** SgnII only (green without red channel). Nuclei are stained blue with bisbenzimide

immunolabeling revealed two distinct spiral ganglion neuronal subpopulations: SgnI (peripherin- negative) neurons that exhibited strong Ngb immunostaining, and SgnII (peripherin-positive) neurons which were not immunostained with Ngb (Fig. 1b). This distinct immunostaining pattern for SgnI and SgnII neurons was confirmed at higher resolution and magnification using DeltaVision Restoration Microscopy System deconvolution images (Fig. 1c–g). Because a small number of SgnII neurons exhibited Ngb immunofluorescence which appeared to exceed background levels, a more quantitative analysis was conducted (see supplemental material). We found that the average cross-sectional area of SgnI neurons was 15 % larger than SgnII neurons, and Ngb fluorescence more intense in SgnI than in SgnII neurons (Supplementary Figs. 3 and 4).

Specific Ngb immunofluorescence was also observed in the stria vascularis (arrow in Fig. 1a) and basilar membrane (arrowhead in Fig. 1a) while no Ngb immunostaining was observed in hair cells, supporting cells, or Schwann cells surrounding SgnI neurons.

In the auditory brainstem, Ngb immunofluorescence was observed in neurons in the superior olivary complex (Fig. 2a–d) and cochlear nucleus (Fig. 2e–g). Throughout the SOC, a substantial portion of neurons were Ngb-immunolabeled. Details on neuron numbers in the SOC are given in Supplementary Table 1. Using the averaged total numbers of neurons in the subnuclei of the rat SOC [53], we calculated the percentage of Ngb-immunoreactive neurons in the respective regions as follows (mean±SD, rounded): lateral superior olive (LSO) 15±6 %, medial superior olive (MSO) 8±1 %, ventral nucleus of the trapezoid body (VNTB) 28±4 %, superior paraolivary nucleus (SPO) 10±2 %, dorsal periolivary nucleus (DPO) 15±2 %, and ventral periolivary nucleus (VPO) 30±3 %). The main cell types labeled in the SOC regions were small bipolar, spindle-shaped neurons oriented dorsoventrally (in the LSO), middle-sized, horizontally oriented bipolar neurons building a small vertical columns between LSO and MNTB (in the MSO), and large, oval to triangular principal neurons (in the MNTB).

Ngb immunofluorescence was also seen (but not quantified) in neuronal cell bodies and fibers within the descending auditory system including auditory cortex, lateral geniculate body, inferior colliculus, and lemniscal nuclei. It was also found in the cochlear nucleus (CN). In sections of the anteroventral CN (AVCN; Fig. 2e, f), Ngb-immunoreactive neuronal perikarya of approximately 18–25 μm soma diameter with one to three apparent processes were observed. According to Pocsai and co-workers [66], these cells most probably are bushy, pyramidal, and small cells. In addition, Ngb-immunoreactive axons were seen within the cochlear nerve (Fig. 2g).

Localization of Ngb-mRNA in Cochlea and Superior Olivary Complex

Ngb-mRNA expression was examined by in situ hybridization (ISH) using antisense and sense Ngb ISH probes (Fig. 3). In mouse cochlea, strong ISH label with the antisense Ngb-probe was localized in the cytoplasm for most of the cells that exhibited characteristic spiral ganglion and Scarpa's (vestibular) ganglion cell body morphology and locations (Fig. 3a). Inner ear sections hybridized with the Ngb sense probe in control ISH experiments were uniformly negative, confirming the specificity of the antisense Ngb probe. While the intensity of the Ngb antisense ISH labeling varied among individual spiral ganglion and Scarpa's ganglion neurons, the ISH technique employed did not permit the discrimination of mRNA transcription levels within specific vestibulocochlear nerve ganglion cell subpopulations (e.g., type I (SgnI) and type II (SgnII) spiral ganglion neurons).

In the mouse and rat SOC (Fig. 3b), hybridization signals were observed in neuronal perikarya of the regions under investigation. The dark-brown ISH reaction-product was also seen in the LSO (Fig. 3c), MSO (Fig. 3d), VNTB, medial nucleus of the trapezoid body (MNTB, Fig. 3e), and in all periolivary regions. The distribution of the hybridization signals was congruent with the location of the immunohistochemical signal with regard to regions and cell types.

Quantification of Ngb-mRNA in Rat SOC and Brain

Ngb-mRNA levels were quantified for selected regions of the rat brain obtained from unfixed material by microdissection using neuropunch needles. Processing by quantitative rt-RT-PCR showed that Ngb-mRNA was elevated more than two-fold in the whole SOC when compared to the level in total brain. Ngb-mRNA levels in cochlear nuclei, cerebral cortex, and cerebellum were similar to that for total brain, while Ngb-mRNA levels in the daytime-sacrificed pineal gland were very low (Fig. 4).

Ngb Immunoreactivity in Identified Olivocochlear Neurons

Following unilateral Fluoro-Gold (FG) injection into the rat scala tympani and retrograde neuronal transport, the tracer was consistently found in cell bodies and processes of the bilateral SOC. On average, 989±75 neuronal somata per animal were labeled in the SOC. They were seen in three topographically separated groups as is typical for OC neurons [62]. Lateral OC (LOC) neurons within the borders of the LSO (Fig. 5a) made up to an average of 53 % of all retrogradely labeled neurons and were predominantly (to 96 %) located ipsilateral to the injection site. The second group of LOC neurons, i.e., shell-neurons, was located around the LSO and in periolivary regions (Fig. 5e) and amounted to 12 % of

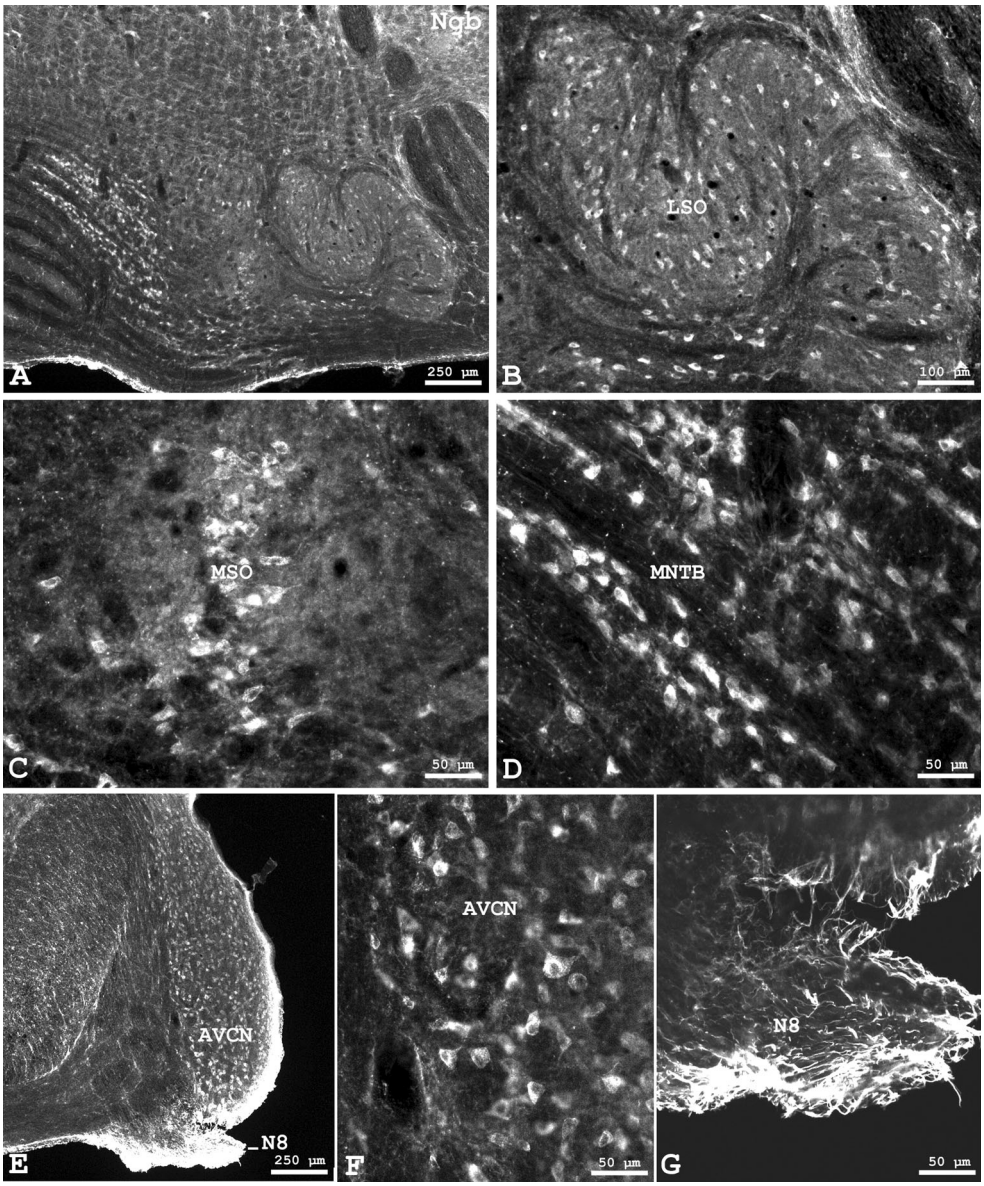

Fig. 2 Neuroglobin (Ngb) protein distribution in the rat superior olivary complex and cochlear nucleus of the rat. **a** Ngb immunofluorescence in different subnuclei of the SOC in the right half of the brainstem. Higher magnifications are given in (**b**) of the lateral superior olive (LSO), in (**c**) of the medial superior olive (MSO), and in (**d**) of the medial nucleus of the trapezoid body (MNTB). **e** Neuroglobin protein distribution in the anteroventral cochlear nucleus (AVCN) and cochlear nerve. Higher magnifications demonstrating positive neuronal perikarya are given in (**f**) of the AVCN and in **g** of the Ngb-immunoractive fibers in the cochlear root of the olivocochlear nerve (N8), shown in extended focal imaging. Orientation in each section is: medial left, dorsal up

retrogradely labeled neurons. The majority (90 %) of shell neurons were located ipsilateral. The third group, i.e., medial olivocochlear (MOC) neurons (Fig. 5c), were seen predominantly in the VNTB, as well as in the RPO, with a contralateral dominance (58 % of labeled MOC neurons). A relatively small number of weakly labeled MOC neurons were observed in the ventral aspect of the posterior part of the MNTB. These data are consistent with previous reports (e.g., [67, 68, 53].

When sections containing retrogradely labeled neurons were subsequently incubated with the Ngb antibody, we found that notable portions (approx. 60 %) of OC neurons were Ngb-positive. Detailed counting (see also Supplementary Table 1) showed that percentages of FG-labeled neurons that were also Ngb-immunoreactive were 48 % in the LSO (Fig. 5b), 72 % in the VNTB (Fig. 5d), 10 % in the SPO, and approximately 75 % in the dorsal and ventral periolivary regions (Fig. 5f).

In contrast, the proportion of FG-labeled neurons within the population of Ngb-immunolabeled neurons in these regions was smaller (19 % in average). In detail, 14 % of the Ngb neurons in the LSO were labeled by FG (and thus were olivocochlear neurons). The respective fractions were 21 % in the VNTB, 7 % in the SPO, 21 % in the DPO, and 30 % in the VPO (Supplementary Table 1).

Double Immunolabeling of nNOS and Ngb in the Mouse Brainstem

In order to further characterize Ngb-positive neurons in the auditory brainstem, we also employed double-immunolabeling for Ngb and neuronal nitric oxide synthase (nNOS), the enzyme responsible for nitric oxide (NO) synthesis in neurons. Frontal sections of the mouse SOC (Fig. 6) exhibited an Ngb-

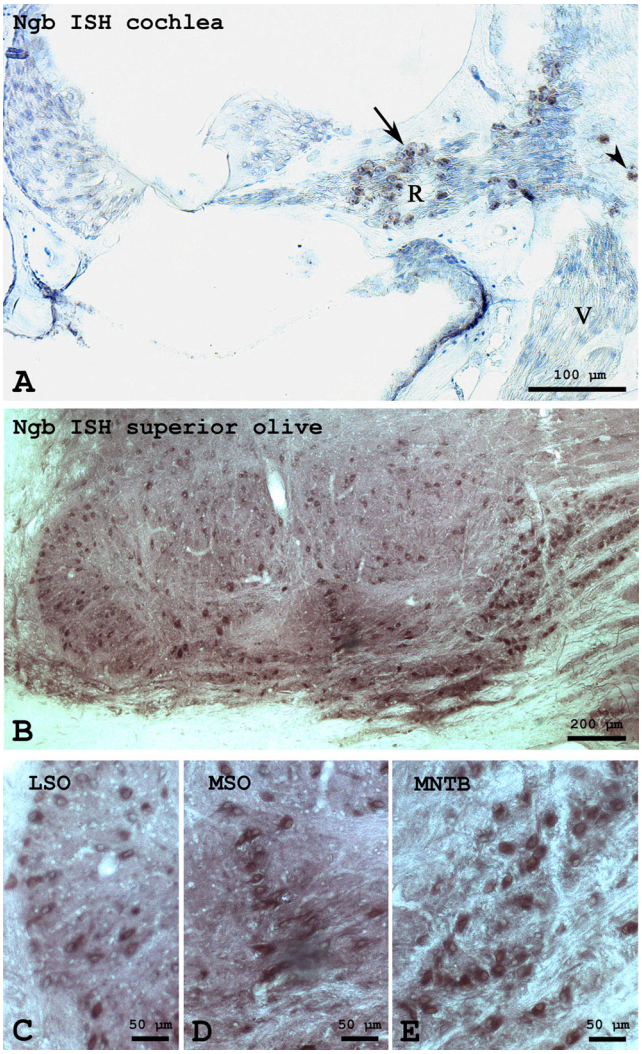

Fig. 3 Neuroglobin in situ hybridization signal (dark reaction product) in cochlea and superior olivary complex. **a** Basal turn section of a mouse cochlea showing Ngb-mRNA in spiral ganglion cells (*arrow*) within Rosenthal's canal (*R*) and Scarpa's ganglion cells (*arrowhead*). The majority of spiral ganglion cells expressed high levels of Ngb-mRNA. No hybridization signals were observed in non-neuronal cells. *V* vestibular branch of the vestibulocochlear (VIIIth) nerve. **b**–**e** Ngb-mRNA in the rat superior olivary complex. Distinct cell groups exhibit the cytoplasmic signal. **b** Overview of the left side of the brainstem. **c** Magnification from the lateral part of the LSO. **d** Magnification showing the MSO. **e** Magnification depicting MNTB neurons

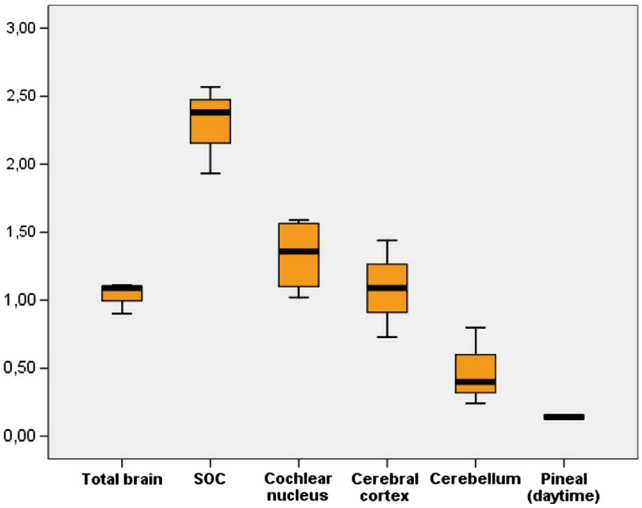

Fig. 4 Quantification by q-RT-PCR of neuroglobin-mRNA in selected regions dissected from rat brain demonstrating the relative high amount of Ngb in the superior olivary complex (SOC). Total brain defined as 1. *Box plots* indicate median, 25 and 75 % percentiles (*horizontal bar* within box, lower, and upper boundary, respectively), 10 and 90 % percentiles (*error bars*)

immunostaining pattern similar to that described above for the rat SOC. Neuronal NOS-immunolabeling in the mouse SOC (Fig. 6b) was expressed less frequently and at lower levels than that for Ngb in the same regions. At higher magnification, some Ngb-immunolabeled neurons in the LSO (Fig. 6c, d; marked by "1") were seen double-labeled for nNOS, while others were not ("2"). Some clusters of large nNOS-immunolabeled neurons were seen in the MNTB (Fig. 6f) of which some exhibited clear Ngb immunoreactivity (Fig. 6e). In the VPO (Fig. 6g, h), Ngb neurons outnumbered nNOS-neurons. In the MNTB, some Ngb-immunolabeled neurons were double-labeled for nNOS ("1"), but the majority was not co-labeled with nNOS ("2").

Ngb Immunolabeling in the Human Brainstem

In order to investigate whether Ngb is also present in the human brainstem, we additionally studied human material stemming from two postmortem brains. These preparations identified the LSO and MSO situated between the abducens and facial nerves in Nissl-stained coronal sections (Supplementary Fig. 6A). Parallel sections, incubated with Ngb-antibody, clearly demonstrated Ngb immunoreactivity in MSO and LSO neurons (Fig. 7). MSO neurons, most of which appeared to be Ngb-immunoreactive, were oriented in a vertical row with their processes extending horizontally (Fig. 7b). Scattered neurons in the LSO (Fig. 7c, d) were labeled by the Ngb antibody, and they were mainly of fusiform shape and oriented vertically.

The Ngb immunostaining in Supplementary Fig. 6 confirms that, in addition to superior olivary structures, the neurons of the nucleus of the facial nerve were Ngb-immunolabeled, while neurons in nuclei of the pons (ventral to the MSO) were not (Supplementary Fig. 6B).

Discussion

Neuroglobin May Support Oxygen Supply to the Inner Ear

Preservation of an adequate oxygen environment in the inner ear is crucial for the maintenance of normal auditory

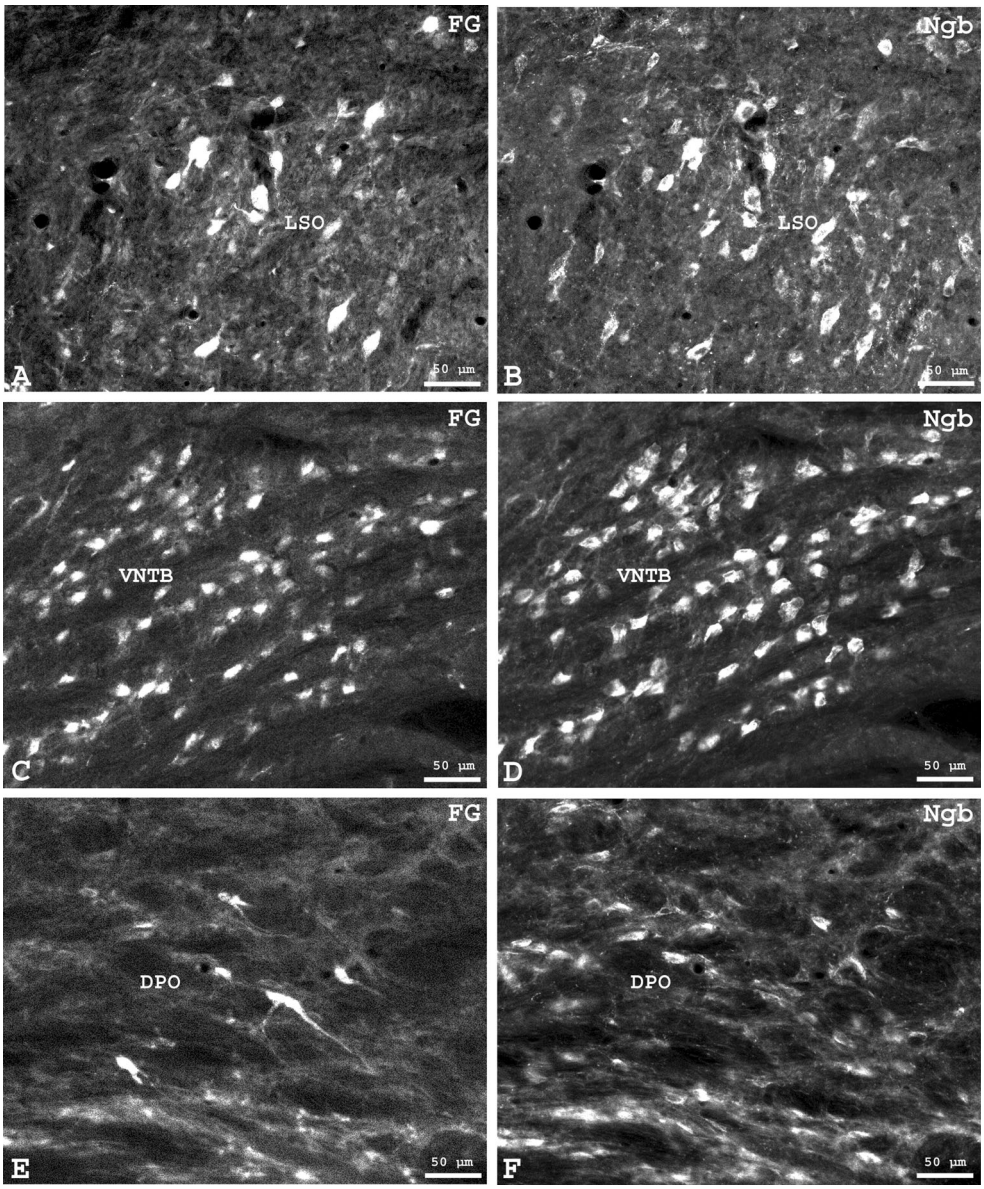

Fig. 5 Labeled neurons in the rat superior olivary complex after injection of **a**, **c**, **e** Fluoro-Gold (FG) into the cochlea and retrograde transport and **b**, **d**, **f** neuroglobin protein distribution (Ngb). Many double-labeled neurons were seen in the **a**, **b** LSO, in the **c**, **d** VNTB, and **e**, **f** dorsal and ventral periolivary nuclei. The Ngb distribution pattern was not affected by cochlear injection

processing, and hypoxia is known to cause rapid and profound hearing pathology [69, 70, 35]. Given the high oxygen demands of signal transduction in the inner ear [41], it is quite remarkable that inner ear neurosensory hair cells lack a direct vascular supply [71]. Instead, the oxidative metabolic requirements of cochlear and vestibular hair cells have to be met entirely by the diffusion of O_2 across relatively large distances. The quest for molecules that may participate in sensing, signaling, storage, or transport of oxygen prompted us to study the distribution of Ngb in the cochlea and its related neural structures. Notably, the distribution of Ngb in the cochlea as observed in this report correlates closely with different neuronal activity-dependent energy demands: cochlear SgnI cells, spontaneously active neurons with fast response kinetics (cf. [72], were highly Ngb-immunoreactive, while SgnII cells, non-spontaneous neurons with slow response kinetics [73], cf. [74] were not. Thus, in the cochlea, Ngb may serve to enhance the O_2 supply in the SgnI cells, neurons which are characterized by their substantial metabolic energy demands and heightened sensitivity to hypoxic/ischemic injury [35].

In addition to neurons, other cell types that have high levels of metabolic activity also require large amounts of O_2. In particular, it is noteworthy that Ngb immunoreactivity was presently observed within the cochlea in the marginal cells of the stria vascularis. These highly active cells possess Na/K-ATPase pumps, which secrete potassium into endolymphatic fluid in order to maintain the cochlear endolymphatic potential [75]. Since Ngb is also expressed in endocrine system secretory cells of anterior pituitary and adrenal glands [15], it is reasonable to assume that Ngb may also help sustain the large amounts of O_2 required by secretory cells of the stria vascularis.

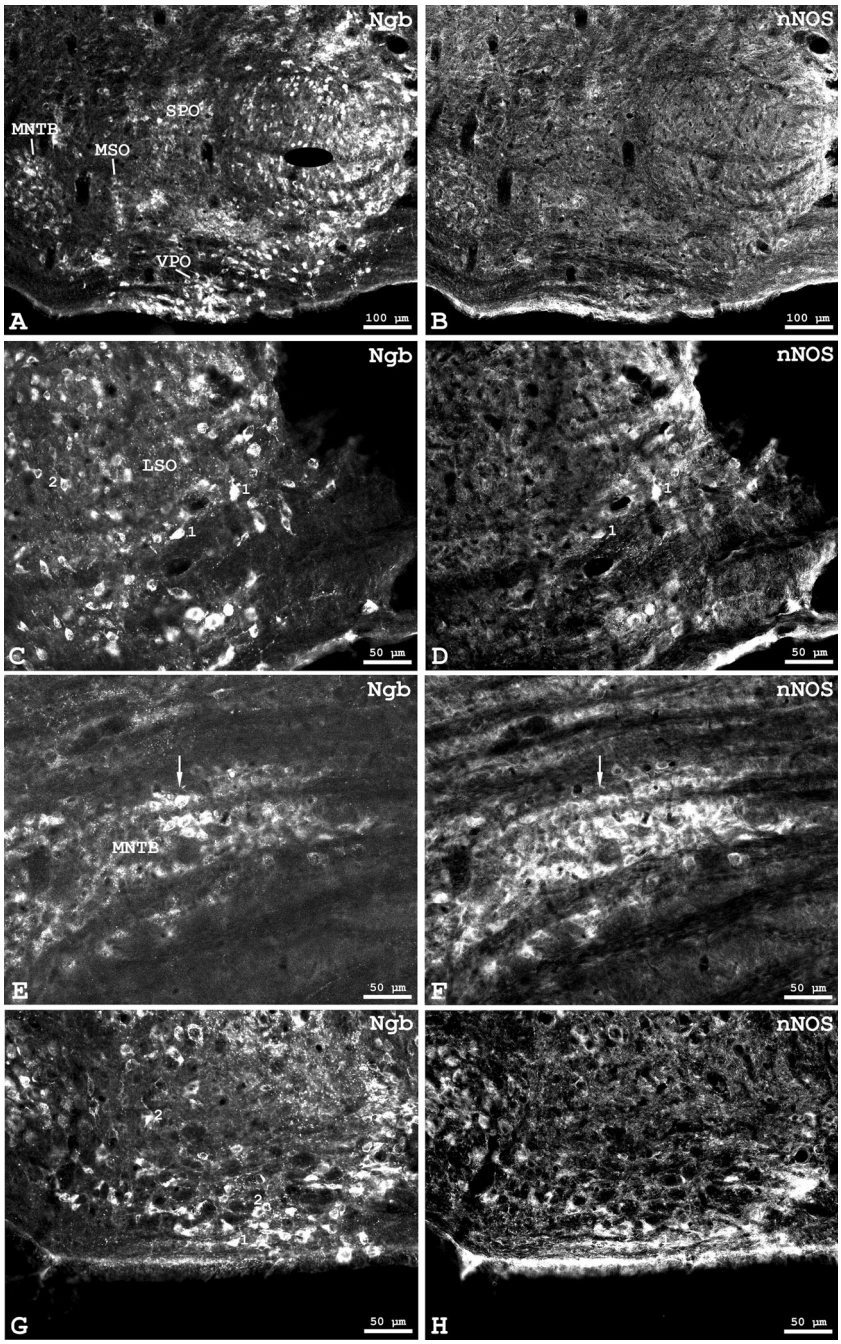

Fig. 6 Double immunofluorescence labeling of **a**, **c**, **e**, **g** neuroglobin (Ngb) and **b**, **d**, **e**, **h** neuronal nitric oxide synthase (nNOS) in frontal sections of the mouse superior olivary complex. **a**, **b** Overview. **c**, **d** Higher magnification of double-labeled neurons (depicted by "1") in the lateral superior olive (LSO). Neurons showing only Ngb immunoreactivity were also found ("2"). Middle is left, dorsal is up. **e**, **f** Higher magnifications from mouse medial nucleus of the trapezoid body (MNTB) where a group of double-labeled neurons is marked by *arrows*, and **g**, **h** in the ventral periolivary region where double-labeled neurons are depicted by "1" and those showing only Ngb immunoreactivity by "2"

To date, the molecular function of Ngb has not been established [33, 34]. However, since Hb and Mb are known to play an important role in O_2 transport and storage, it has been postulated that Ngb might serve a Mb-like function in neurons by facilitating the delivery of O_2 to mitochondria [3]. This notion is further supported by the fact that the affinity of Ngb for O_2 is in same range as that of vertebrate Mb (i.e., approximately 1–2 Torr) [76] and by evidence that the distribution of Ngb protein within highly-active cells correlates closely with sites where mitochondria congregate [25, 26, 18]. Unfortunately, definitive quantitative data on Ngb-mRNA expression levels in individual cells are still lacking, but the available data suggests that any Ngb-mediated mechanism which serves to increase the O_2 supply of SgnI cells would help compensate for the diffusion-limited delivery of oxygen within the cochlea during periods of hypoxia. Notably, while Ngb is found in large populations of neurons dispersed throughout the brain, the expression of Ngb-mRNA and protein is sometimes not coincident, and the specific pattern of Ngb transcription and translation is dependent upon particular brain regions and cell types [15–24].

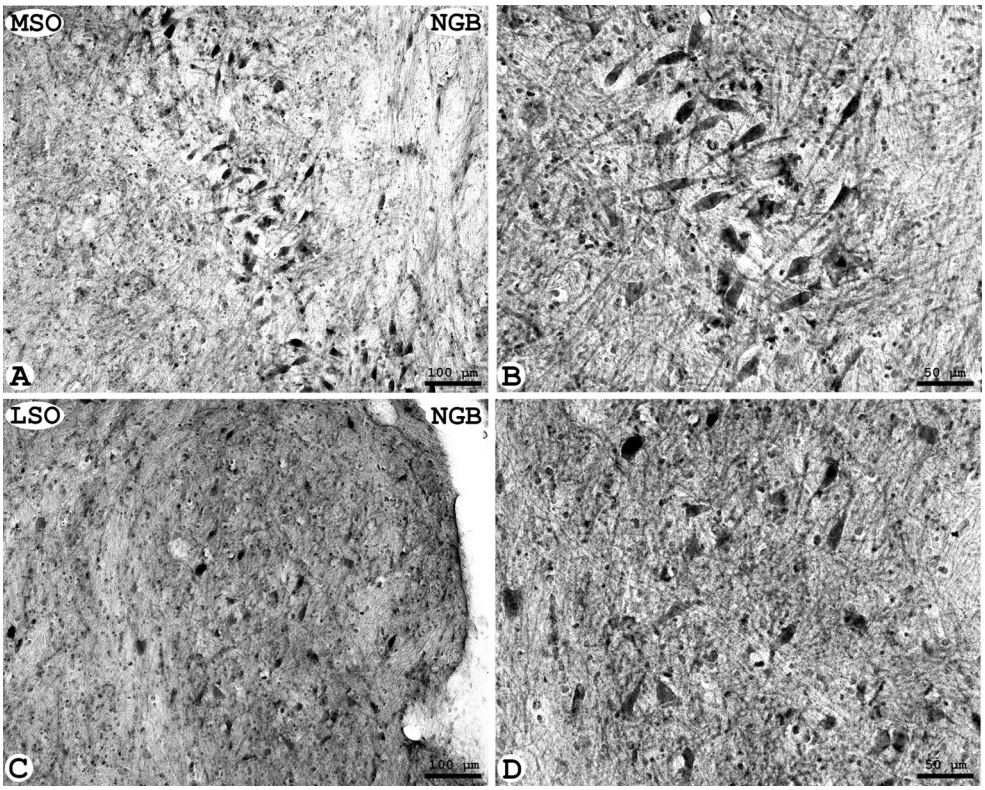

Fig. 7 Neuroglobin protein distribution (Ngb) in a frontal section of the human superior olivary complex (for localization of the nuclei, see Supplementary Fig. 6) at low and higher power magnification in **a**, **b** the medial superior olive (MSO) and **c**, **d** the lateral superior olive (LSO)

Neuroglobin Expression Differentiates Type I from Type II Spiral Ganglion Neurons

At a practical level, the distinct nature of the Ngb immunostaining patterns provides a novel means for distinguishing SgnI cells from SgnII cells. Because the functional role of SgnII cells in the mammalian cochlea is still poorly understood, questions remain about how to interpret the significance of the differential expression of Ngb in the two spiral ganglion cell subpopulations. Although more than four decades have elapsed since Spoendlin discovered that 95 % of primary auditory neurons (i.e., SgnI cells) provide exclusive afferent innervation for the single row of IHCs (and thus play the major role in transmitting auditory information from the inner ear into the CNS) and that the remaining 5 % of primary auditory neurons (i.e., SgnII cells) provide the only afferent innervation for the three rows of OHCs [77], at this time, we still know little about SgnII cells beyond their anatomic features and projection patterns. However, interest in the function of SgnII cells increased after it was discovered that the OHCs they innervate possess unique electromotile responses: OHC stimulation induces high-speed modulation of their somatic length, cellular changes which act as a mechanical "cochlear amplifier" that enhances cochlear sensitivity, specificity, and signal strength [78]. While our mouse data were in substantial agreement with earlier reports that rat SgnI cells have larger perikarya than SgnII cells [65], the fact that the size distributions for the two spiral ganglion cell subpopulations overlap extensively (Supplementary Fig. 3) suggest that any functional differences between SgnI and SgnII cells are reflected less by gross cell anatomy and more by cellular metabolic mechanisms.

Given that IHC afferents comprised of SgnI neurons express Ngb, while OHC afferents are made up of SgnII neurons that do not express Ngb, the question arises as to whether brainstem neurons innervating OHCs express Ngb. Notably, OHCs receive direct efferent innervation from olivocochlear neurons in the superior olivary complex, which constitutes the first binaural hearing center in the ascending auditory pathway. In the present study, many neurons of the SOC were shown to express Ngb-mRNA and protein.

Neuroglobin Expression by Olivocochlear Neurons

In order to confirm that identified olivocochlear neurons are Ngb-immunoreactive, we injected the retrograde neuronal tracer FG into the scala tympani of rats. After uptake by terminals and retrograde transport of FG, we found labeled neurons in the bilateral SOC, with numbers and distribution consistent with previous reports (e.g., [67, 68, 53]. By combining FG-tracing and Ngb immunohistochemical staining, we found that approximately 60 % of the FG-labeled olivocochlear neurons expressed Ngb. Notably, the OCN can be divided into lateral (LOC) and medial (MOC) olivocochlear neurons. The cell bodies of the former are located in or around the LSO and their axons provide efferent synapses onto IHC afferents,

whereby they modulate the glutamatergic IHC-afferent terminal synapses, and thus serve to regulate SgnI activity in response to sound stimulation (cf. [79].

In contrast to LOCs, the MOC neuron cell bodies are located in the ventral nucleus of the trapezoid body (VNTB) and rostral periolivary area (RPO), and their axons provide efferent synapses directly onto the OHCs [80, 62, 81–83], for review see [84]. MOC activity has been shown to elicit outer hair cell mechanical effects, which modulate otoacoustic emissions and can provide protection against acoustic injury (cf. [85, 86]. In this study, we found that both LOC and MOC neurons express Ngb. Given the important role of the SOC in protecting hair cells from sound-induced damage, it may be assumed that Ngb expression in LOC and MOC neurons that have high discharge rates [87] and energy demands would help them physiologically during periods of noise-induced oxidative stress.

Possible Interaction Between Neuroglobin and Nitric Oxide

The specialized anatomy and physiology of the cochlea and its related neural structures may provide unique insights into the possible function of Ngb. For instance, it has been suggested that Ngb might scavenge nitric oxide (NO) [88, 89], which is produced following the activation of nitric oxide synthase (NOS) during hypoxia, and other forms of environmental stress [2].

The possibility of NO scavenging by Ngb is supported by earlier reports of neuronal NOS (nNOS) in the peripheral and central auditory system [90, 53, 91], and our evidence for the co-expression of nNOS [53] and Ngb (this report) in the majority of spiral ganglion neurons (i.e., SgnI cells), and in mouse and rat SOC neurons (this report). In addition, there is also an evidence of a substantial overlap in the constitutive expression patterns for Ngb [15] and nNOS [92] in non-auditory regions of the brain.

Finally, further evidence of possible interactions between Ngb and NO in the central nervous system has previously been provided by our group (cf. [34, 93], and by the observed co-expression of Ngb and nNOS in the rat hypothalamus [94].

Cellular Distribution and Localization of Neuroglobin

The present results demonstrate, by means of various methods, that neuroglobin is present in neuronal cells of the cochlea and the auditory brainstem. Notably, Ngb immunolabeling was not observed in Schwann cells (i.e., myelin-producing cells enveloping SgnI cells) or CNS astrocytes. Ngb expression in CNS glial cells has only been observed in species which live in oxygen-challenged environments such as the subterranean mole rat Spalax, as well as seals and whales [24, 18, 20].

The comparison between the immunohistochemical and ISH-results revealed substantial agreement between the Ngb-immunostaining and mRNA-expression patterns in the superior olivary complex of the brainstem (this report) in spiral ganglion neurons in the present and in an earlier study [51] as well as in Scarpa's ganglion neurons (this report). However, the presence of Ngb protein in the absence of antisense mRNA-Ngb-hybridization in stria vascularis and the basilar membrane suggests that Ngb either is transcribed in these tissues at levels below the sensitivity of our ISH assays or it is transported to these sites after translation. In addition, the relatively weak Ngb protein bands from cochlea lysates (see Supplementary Figs. 1 and 2) are probably due to the fact that neurons constitute only a relatively small fraction of the total cellular volume of the cochlea. Thus, it can be assumed that neurons in the cochlea (and in brain regions with relatively few neuronal somata) express considerably more Ngb-mRNA and protein than would be expected from the estimates obtained using the whole cochlea or brain tissue.

It should be noted that in the SOC 10–30 % of the neurons are Ngb-positive. Nineteen percent of these Ngb-neurons were olivocochlear neurons. It is currently unknown whether Ngb-positive SOC neurons possess a common feature such as high energy demand and/or whether they are anatomically or physiologically connected, but it appears that the SOC with its various functions in the hearing processes has the unspecified advantage of Ngb-producing neurons. Our quantitative rt-RT-PCR data determined that Ngb-mRNA levels were significantly higher in the SOC than those for total brain, which further supports the hypothesis that Ngb may play a special role in the peripheral and central auditory nervous system.

In the cochlear nucleus (CN), Ngb-mRNA levels were in approximately the same range as in total brain. Immunostaining with Ngb-antibody was confined to small and middle-sized somata scattered throughout the CN. Fibers of the cochlear nerve (i.e., axons of spiral ganglion neurons) terminate in the CN, which serves as first relay center in the ascending auditory pathway. From the variety of cell types previously described in rat CN, the observed cell distribution, soma size, and processes of Ngb-labeled neurons suggest that most were bushy cells, pyramidal cells, or small cells [66]. These types of CN cells project centrally to the SOC, inferior colliculus (IC), and medial geniculate body (MGB) (cf. [61].

Ngb-immunoreactive neurons were observed in the IC, MGB, lemniscal nuclei, and auditory cortex as parts of the descending auditory system, which, judging from cell shape, size, and distribution, project itself to the LSO, periolivary regions, lateral lemniscus, and the IC. Although we did not quantify neuroglobin in these regions yet, it appears that the expression levels did not exceed those in other brain regions.

Taken together, our cochlea and brainstem data show that IHCs are contacted by Ngb-expressing SgnI afferent neurons, while OHCs are contacted by Ngb-expressing efferent neurons. Although we do not know yet what the local role of Ngb is, it is significant that both types of hair cell are contacted by

Ngb-expressing neurons. Thus, it is possible that Ngb may play an active role in the transport or storage of oxygen in auditory neurons, and that Ngb may also provide protection for the auditory nervous system under conditions when energy demands are high. In addition, Ngb may also act as signal molecule in oxygen sensing. In any case, if Ngb-expressing afferent and efferent auditory system neurons do exert a direct Ngb-involving influence on cochlear hair cells, then the mechanism would presumably involve Ngb-transport from neuronal soma to peripheral processes, in particular to the axon endings. The question as to whether Ngb is present in distal parts of neurons has not previously been discussed. While some evidence of Ngb protein within axons can be found in the figures from prior immunohistochemical studies of the dorsal root ganglion and in dorsal spinal cord [95] and an investigation of the central projections of the optic nerve [96], our present observations that Ngb-immunoreactive vestibulocochlear nerve axons project from the cochlea into the brainstem cochlear nucleus (Fig. 2e, g) have confirmed for the first time that Ngb can be transported within axonal processes over relatively long distances.

Finally, to extend our comparative understanding of Ngb expression in the SOC, we included an investigation of brainstem slices from human postmortem brains. In frontal sections, the human SOC was located between abducens and facial nerves (see Supplementary Fig. 6), in agreement with the literature (cf. [97, 98]. Notably, within the human SOC, many MSO neurons, and scattered neurons in the LSO, were Ngb-immunoreactive, similar to the situation seen in both the mouse and rat. Other neuronal groups at this brainstem level exhibited differential Ngb staining insofar as neurons of the facial nucleus were positive while neurons of the nuclei of the pons were Ngb-negative.

Conclusions

Our study provides the first detailed analysis of Ngb expression in the cochlea and superior olivary complex of the auditory brainstem. We demonstrate, by a variety of experimental methods, that Ngb is highly expressed in mouse and rat spiral ganglion type I neurons, and in the SOC of rats, mice, and men. Further studies, however, are required to elucidate the specific role of Ngb within various sensory (e.g., visual, auditory, and vestibular) systems under normal and pathological conditions. Ngb has been shown to protect neurons from hypoxic-ischemic injury [30, 31, 33, 34], which suggests that a better understanding of the role of Ngb in the inner ear and auditory brainstem may provide the basis for new clinical approaches to treat, prevent, and diagnose cochlear oxidative stress, a leading cause of sensorineural hearing loss (SNHL) for which, at present, no effective therapeutics exist.

Acknowledgments This work was supported by grants from the National Institutes of Health, National Institute for Deafness and Communication Disorders grants DC00386 and DC02666, and the Research Service of the Department of Veterans Affairs (USA), from the Röttger-Stiftung and Hoffmann-Klose-Stiftung (Germany) and by the Deutsche Forschungsgemeinschaft (Bu956/5 and Ha2103/3). We thank Dr. Thorsten Fink, Department of Pathology, HSK Wiesbaden, Germany, for providing the human brainstem specimens. The University of California Cancer Center Biomedical Imaging Core is also thanked for their imaging support. We thank Steve McMullen of the UCSD Cancer Center Digital Imaging Shared Resource for his assistance in collecting the deconvolution digital microscope images; Anuradha Desai of the Department of Surgery, University of California at San Diego and the Veterans Affairs Research Service, VA San Diego Healthcare System, CA, for her technical assistance with the Western blot assays; and Kunlin Jin and David A. Greenberg of Buck Institute for Age Research, Novato, CA, for their helpful discussions and comments.

Conflict of Interest The authors declare that they have no conflict of interest.

References

1. Weber RE, Vinogradov SN (2001) Nonvertebrate hemoglobins: functions and molecular adaptations. Physiol Rev 81(2):569–628
2. Wittenberg JB, Wittenberg BA (2003) Myoglobin function reassessed. J Exp Biol 206(Pt 12):2011–2020
3. Burmester T, Weich B, Reinhardt S, Hankeln T (2000) A vertebrate globin expressed in the brain. Nature 407:520–523
4. Trent JT, Hargrove MS (2002) A ubiquitously expressed human hexacoordinate hemoglobin. J Biol Chem 277:19538–19545
5. Kawada N, Kristensen DB, Asahina K, Nakatani K, Minamiyama Y, Seki S, Yoshizato K (2001) Characterization of a stellate cell activation-associated protein (STAP) with peroxidase activity found in rat hepatic stellate cells. J Biol Chem 276:25318–25323
6. Burmester T, Ebner B, Weich B, Hankeln T (2002) Cytoglobin: a novel globin type ubiquitously expressed in vertebrate tissues. Mol Biol Evol 19(4):416–421
7. Kugelstadt D, Haberkamp M, Hankeln T, Burmester T (2004) Neuroglobin, cytoglobin, and a novel, eye-specific globin from chicken. Biochem Biophys Res Commun 325:719–725
8. Roesner A, Fuchs C, Hankeln T, Burmester T (2005) A globin gene of ancient evolutionary origin in lower vertebrates: evidence for two distinct globin families in animals. Mol Biol Evol 22:12–20
9. Fuchs C, Burmester T, Hankeln T (2006) The amphibian globin gene repertoire as revealed by the Xenopus genome. Cytogenet Genome Res 112(3–4):296–306
10. Hoogewijs D, Ebner B, Germani F, Hoffmann FG, Fabrizius A, Moens L, Burmester T, Dewilde S, Storz JF, Vinogradov SN, Hankeln T (2012) Androglobin: a chimeric globin in metazoans that is preferentially expressed in mammalian testes. Mol Biol Evol 29(4): 1105–1114
11. Burmester T, Hankeln T (2014) Function and evolution of vertebrate globins. Acta Physiol 211:501–514
12. Schwarze K, Burmester T (2013) Conservation of globin genes in the "living fossil" *Latimeria chalumnae* and reconstruction of the evolution of the vertebrate globin family. Biochim Biophys Acta 1834(9): 1801–1812
13. Burmester T, Haberkamp M, Mitz S, Roesner A, Schmidt M, Ebner B, Gerlach F, Fuchs C, Hankeln T (2004) Neuroglobin and cytoglobin: genes, proteins and evolution. IUBMB Life 56:703–707
14. Geuens E, Brouns I, Flamez D, DeWilde S, Timmermans JP, Moens L (2003) A globin in the nucleus! J Biol Chem 278:30417–30420

15. Reuss S, Saaler-Reinhardt S, Weich B, Wystub S, Reuss MH, Burmester T, Hankeln T (2002) Expression analysis of neuroglobin mRNA in rodent tissues. Neuroscience 115:645–656
16. Wystub S, Laufs T, Schmidt M, Burmester T, Maas U, Saaler-Reinhardt S, Hankeln T, Reuss S (2003) Localisation of neuroglobin protein in the mouse brain. Neurosci Lett 346:114–116
17. Laufs TL, Wystub S, Reuss S, Burmester T, SaalerReinhardt S, Hankeln T (2004) Neuron-specific expression of neuroglobin in mammals. Neurosci Lett 362:83–86
18. Mitz SA, Reuss S, Folkow LP, Blix AS, Ramirez JM, Hankeln T, Burmester T (2009) When the brain goes diving: glial oxidative metabolism may confer hypoxia tolerance to the seal brain. Neuroscience 163:552–560
19. Hundahl CA, Allen GC, Nyengaard JR, Dewilde S, Carter BD, Kelsen J, Hay-Schmidt A (2008) Neuroglobin in the rat brain: localization. Neuroendocrinology 88:173–182
20. Schneuer M, Flachsbarth S, Czech-Damal NU, Folkow LP, Siebert U, Burmester T (2012) Neuroglobin of seals and whales: evidence for a divergent role in the diving brain. Neuroscience 223:35–44
21. Mammen PPA, Shelton JM, Goetsch SC, Williams SC, Richardson JA, Garry MG, Garry DJ (2002) Neuroglobin, a novel member of the globin family, is expressed in focal regions of the brain. J Histochem Cytochem 50:1591–1598
22. Hundahl CA, Allen GC, Hannibal J, Kjaer K, Rehfeld JF, Dewilde S, Nyengaard JR, Kelsen J, Hay-Schmidt A (2010) Anatomical characterization of cytoglobin and neuroglobin mRNA and protein expression in the mouse brain. Brain Res 1331:58–73
23. Schmidt M, Laufs T, Reuss S, Hankeln T, Burmester T (2005) Divergent distribution of cytoglobin and neuroglobin in the murine eye. Neurosci Lett 374:207–211
24. Avivi A, Gerlach F, Joel A, Reuss S, Burmester T, Nevo E, Hankeln T (2010) Neuroglobin, cytoglobin, and myoglobin contribute to hypoxia adaptation of the subterranean mole rat Spalax. Proc Natl Acad Sci U S A 107(50):21570–21575
25. Schmidt M, Giessl A, Laufs T, Hankeln T, Wolfrum U, Burmester T (2003) How does the eye breathe?—Evidence for neuroglobin-mediated oxygen supply in the mammalian retina. J Biol Chem 278:1932–1935
26. Bentmann A, Schmidt M, Reuss S, Wolfrum U, Hankeln T, Burmester T (2005) Divergent distribution in vascular and avascular mammalian retinae links neuroglobin to cellular respiration. J Biol Chem 280:20660–20665
27. Ostojic J, Sakaguchi DS, de Lathouder Y, Hargrove MS, Trent JT 3rd, Kwon YH, Kardon RH, Kuehn MH, Betts DM, Grozdanic S (2006) Neuroglobin and cytoglobin: oxygen-binding proteins in retinal neurons. Invest Ophthalmol Vis Sci 47(3):1016–1023
28. Rajendram R, Rao NA (2007) Neuroglobin in normal retina and retina from eyes with advanced glaucoma. Br J Ophthalmol 91(5): 663–666
29. Roesner A, Mitz SA, Hankeln T, Burmester T (2008) Globins and hypoxia adaptation in the goldfish, Carassius auratus. FEBS J 275(14):3633–3643
30. Sun Y, Jin K, Mao XO, Zhu Y, Greenberg DA (2001) Neuroglobin is upregulated by and protects neurons from hypoxic-ischemic injury. Proc Natl Acad Sci U S A 98:15306–15311
31. Sun YJ, Jin KL, Peel A, Mao XO, Xie L, Greenberg DA (2003) Neuroglobin protects the brain from experimental stroke in vivo. Proc Natl Acad Sci U S A 100:3497–3500
32. Raida Z, Hundahl CA, Kelsen J, Nyengaard JR, Hay-Schmidt A (2012) Reduced infarct size in neuroglobin-null mice after experimental stroke in vivo. Exp Translat Stroke Med 4(1):15
33. Burmester T, Hankeln T (2009) What is the function of neuroglobin? J Exp Biol 212(Pt 10):1423–1428
34. Hankeln T, Ebner B, Fuchs C, Gerlach F, Haberkamp M, Laufs TL, Roesner A, Schmidt M, Weich B, Wystub S, Saaler-Reinhardt S, Reuss S, Bolognesi M, Sanctis DD, Marden MC, Kiger L, Moens L, Dewilde S, Nevo E, Avivi A, Weber RE, Fago A, Burmester T (2005) Neuroglobin and cytoglobin in search of their role in the vertebrate globin family. J Inorg Biochem 99:110–119
35. Koga K, Hakuba N, Watanabe F, Shudou M, Nakagawa T, Gyo K (2003) Transient cochlear ischemia causes delayed cell death in the organ of Corti: an experimental study in gerbils. J Comp Neurol 456: 105–111
36. Brown MC, Santos-Sacchi J (2013) Audition. In: Squire L, Berg D, Bloom FE, du Lac S, Ghosh A (eds) Fundamental Neuroscience, 4th edn. Elsevier, Amsterdam, pp 553–576
37. Slepecky NB (1996) Structure of the mammalian cochlea. In: Dallos P, Popper AN, Fay RR (eds) The Cochlea, vol 8, Springer Handbook of Auditory Research. Springer, New York, pp 44–129
38. Dallos P (1996) Overview: cochlear neurobiology. In: Dallos P, Popper AN, Fay RR (eds) The Cochlea, vol 8. Springer Handbook of Auditory Research. Springer, New York, pp 1–43
39. Møller A (2007) Hearing: anatomy, physiology, and disorders of the auditory system, 2nd edn. Elsevier, Amsterdam
40. Raphael Y, Altschuler RA (2003) Structure and innervation of the cochlea. Brain Res Bull 60:397–422
41. Puschner B, Schacht J (1997) Energy metabolism in cochlear outer hair cells in vitro. Hear Res 114(1–2):102–106
42. Ryan AF, Goodwin P, Woolf NK, Sharp F (1982) Auditory stimulation alters the pattern of 2-deoxyglucose uptake in the inner ear. Brain Res 234(2):213–225
43. Goodwin PC, Ryan AF, Sharp FR, Woolf NK, Davidson TM (1984) Cochlear deoxyglucose uptake: relationship to stimulus intensity. Hearing Res 15(3):215–224
44. Canlon B, Anniko M (1987) The postnatal development of stimulated deoxyglucose uptake into the mouse cochlea and the inferior colliculus. Archives of oto-rhino-laryngology 244(5):273–277
45. Schousboe A, Booher J, Hertz L (1970) Content of ATP in cultivated neurons and astrocytes exposed to balanced and potassium-rich media. J Neurochem 17(10):1501–1504
46. Thalmann R, Thalmann I, Comegys TH (1972) Quantitative cytochemistry of the organ of Corti. Dissection, weight determination and analysis of single outer hair cells. Laryngoscope 82(11):2059–2078
47. Thalmann R, Miyoshi T, Thalmann I (1972) The influence of ischemia upon the energy reserves of inner ear tissues. Laryngoscope 82(12):2249–2272
48. Scheibe F, Haupt H, Rothe E, Hache U (1981) On the glucose, pyruvate, and lactate concentration of perilymph, blood, and cerebrospinal fluid of unexposed and sound-exposed guinea pigs under ethyl urethane anesthesia (author's transl). Archives of oto-rhino-laryngology 233(1):89–97
49. Axelsson A (1988) Comparative anatomy of cochlear blood vessels. Am J Otolaryngol 9(6):278–290
50. Yu DY, Cringle SJ (2001) Oxygen distribution and consumption within the retina in vascularised and avascular retinas and in animal models of retinal disease. Progr Retinal Eye Res 20(2):175–208
51. Lopez IA, Acuna D, Shahram Y, Mowlds D, Ngan AM, Rungvivatjarus T, Sharma Y, Edmond J (2010) Neuroglobin expression in the cochlea of rat pups exposed to chronic very mild carbon monoxide (25 ppm) in air during and after the prenatal period. Brain Res 1327:56–68
52. McLean IW, Nakane PK (1974) Periodate-lysine-paraformaldehyde fixative. A new fixation for immunoelectron microscopy. J Histochem Cytochem 22:1077–1083
53. Riemann R, Reuss S (1999) Nitric oxide synthase in identified olivocochlear projection neurons in rat and guinea pig. Hear Res 135:181–189
54. Reuss S, Disque-Kaiser U, Antoniou-Lipfert P, Najaf Gholi M, Riemann E, Riemann R (2009) Neurochemistry of olivocochlear neurons in the hamster. Anat Rec 292:461–471
55. Abercrombie M (1946) Estimation of nuclear population from microtome sections. Anat Rec 94:239–247

56. Paxinos G, Franklin KBJ (2001) The mouse brain in stereotaxic coordinates, 2nd edn. Academic, San Diego
57. Paxinos G, Watson C (2007) The rat brain in stereotaxic coordinates, 4th edn. Academic, San Diego
58. Schwartz IR (1992) The superior olivary complex and lateral lemniscal nuclei. In: Webster DB, Popper AN, Fay RF (eds) The Mammalian Auditory Pathway: Neuroanatomy. Springer, New York, pp 117–167
59. Warr BW (1992) Organization of olivocochlear efferent systems in mammals. In: Webster DB, Popper AN, Fay RR (eds) The mammalian auditory pathway. Neuroanatomy Springer, New York, pp 410–448
60. Kulesza RJ, Vinuela A, Saldana E, Berrebi AS (2002) Unbiased stereological estimates of neuron number in subcortical auditory nuclei of the rat. Hear Res 168:12–24
61. Malmierca MS, Merchan MA (2004) Auditory system. In: Paxinos G (ed) The rat nervous system, Thirdth edn. Elsevier Academic Press, Amsterdam, pp 997–1082
62. Vetter DE, Mugnaini E (1992) Distribution and dendritic features of three groups of rat olivocochlear neurons. A study with two retrograde cholera toxin tracers. Anat Embryol 185:1–16
63. Hsu SM, Raine L, Fanger H (1981) Use of avidin-biotin-peroxidase complex (ABC) in immunoperoxidase techniques: a comparison between ABC and unlabeled antibody (PAP) procedures. J Histochem Cytochem 29:577–580
64. Berglund AM, Ryugo DK (1991) Neurofilament antibodies and spiral ganglion neurons of the mammalian cochlea. J Comp Neurol 306(3):393–408
65. Hafidi A (1998) Peripherin-like immunoreactivity in type II spiral ganglion cell body and projections. Brain Res 805:181–190
66. Pocsai K, Pal B, Pap P, Bakondi G, Kosztka L, Rusznak Z, Szucs G (2007) Rhodamine backfilling and confocal microscopy as a tool for the unambiguous identification of neuronal cell types: a study of the neurones of the rat cochlear nucleus. Brain Res Bull 71(5):529–538
67. White JS, Warr WB (1983) The dual origins of the olivocochlear bundle in the albino rat. J Comp Neurol 219:203–214
68. Aschoff A, Ostwald J (1988) Distribution of cochlear efferents and olivo-collicular neurons in the brainstem of rat and guinea pig. A double labeling study with fluorescent tracers. Exp Brain Res 71: 241–251
69. Sawada S, Mori N, Mount RJ, Harrison RV (2001) Differential vulnerability of inner and outer hair cell systems to chronic mild hypoxia and glutamate ototoxicity: insights into the cause of auditory neuropathy. J Otolaryngol 30(2):106–114
70. Nakashima T, Naganawa S, Sone M, Tominaga M, Hayashi H, Yamamoto H, Liu XL, Nuttall AL (2003) Disorders of cochlear blood flow. Brain Res Rev 43:17–28
71. Axelsson A, Ryan A, Woolf N (1986) The early postnatal development of the cochlear vasculature in the gerbil. Acta Otolaryngol 101(1–2):75–87
72. Taberner AM, Liberman MC (2005) Response properties of single auditory nerve fibers in the mouse. J Neurophysiol 93(1):557–569
73. Robertson D (1984) Horseradish peroxidase injection of physiologically characterized afferent and efferent neurones in the guinea pig spiral ganglion. Hear Res 15(2):113–121
74. Rusznak Z, Szucs G (2009) Spiral ganglion neurones: an overview of morphology, firing behaviour, ionic channels and function. Pflugers Archiv: Eur J Physiol 457(6):1303–1325
75. Xia A, Kikuchi T, Hozawa K, Katori Y, Takasaka T (1999) Expression of connexin 26 and Na, K-ATPase in the developing mouse cochlear lateral wall: functional implications. Brain Res 846:106–111
76. Dewilde S, Kiger L, Burmester T, Hankeln T, Baudin-Creuza V, Aerts T, Marden MC, Caubergs R, Moens L (2001) Biochemical characterization and ligand binding properties of neuroglobin, a novel member of the globin family. J Biol Chem 276(42):38949–38955
77. Spoendlin H (1972) Innervation densities of the cochlea. Acta Otolaryngol 73(2):235–248
78. Brownell WE, Bader CR, Bertrand D, de Ribaupierre Y (1985) Evoked mechanical responses of isolated cochlear outer hair cells. Science 227(4683):194–196
79. Ruel J, Wang J, Rebillard G, Eybalin M, Lloyd R, Pujol R, Puel JL (2007) Physiology, pharmacology and plasticity at the inner hair cell synaptic complex. Hear Res 227(1–2):19–27
80. Warr WB, Boche JB, Neely ST (1997) Efferent innervation of the inner hair cell region: origins and terminations of two lateral olivocochlear systems. Hear Res 108:89–111
81. Horvath M, Kraus KS, Illing RB (2000) Olivocochlear neurons sending axon collaterals into the ventral cochlear nucleus of the rat. J Comp Neurol 422:95–105
82. Sanchez-Gonzalez MA, Warr WB, Lopez DE (2003) Anatomy of olivocochlear neurons in the hamster studied with Fluoro-Gold. Hear Res 185:65–76
83. Hill JC, Prasher DK, Luxon LM (1997) Evidence for efferent effects on auditory afferent activity, and their functional relevance. Clin Otolaryngol Alied Sci 22(5):394–402
84. Guinan JJ Jr (2010) Cochlear efferent innervation and function. Curr Opin Otolaryngol Head Neck Surge 18(5):447–453
85. Wersinger E, Fuchs PA (2011) Modulation of hair cell efferents. Hear Res 279(1–2):1–12
86. Guinan JJ Jr, Salt A, Cheatham MA (2012) Progress in cochlear physiology after Bekesy. Hear Res 293(1–2):12–20
87. Liberman MC (1988) Response properties of cochlear efferent neurons: monaural vs. binaural stimulation and the effects of noise. J Neurophysiol 60(5):1779–1798
88. Brunori M, Giuffre A, Nienhaus K, Nienhaus GU, Scandurra FM, Vallone B (2005) Neuroglobin, nitric oxide, and oxygen: functional pathways and conformational changes. Proc Natl Acad Sci U S A 102:8483–8488
89. Brunori M, Vallone B (2007) Neuroglobin, seven years after. Cell Mol Life Sci 64:1259–1268
90. Fessenden JD, Altschuler RA, Seasholtz AF, Schacht J (1999) Nitric oxide/cyclic guanosine monophosphate pathway in the peripheral and central auditory system of the rat. J Comp Neurol 404:52–63
91. Zdanski CJ, Prazma J, Petrusz P, Grossman G, Raynor E, Smith TL, Pillsbury HC (1994) Nitric oxide synthase is an active enzyme in the spiral ganglion cells of the rat cochlea. Hear Res 79:39–47
92. Rodrigo J, Springall DR, Uttenthal O, Bentura ML, Abadia-Molina F, Riveros-Moreno V, Martínez-Murillo R, Polak JM, Moncada S (1994) Localization of nitric oxide synthase in the adult rat brain. Philos Trans R Soc Lond B Biol Sci 345:175–221
93. Burmester T, Hankeln T (2008) Neuroglobin and other nerve hemoglobins. In: Bolognesi M, di Prisco G, Verde C (eds) Dioxygen Binding and Sensing Proteins, vol 9. Protein Reviews. Springer, Milan, pp 211–222
94. Hundahl CA, Kelsen J, Dewilde S, Hay-Schmidt A (2008) Neuroglobin in the rat brain (II): co-localisation with neurotransmitters. Neuroendocrinology 88:183–198
95. Hankeln T, Wystub S, Laufs T, Schmidt M, Gerlach F, Saaler-Reinhardt S, Reuss S, Burmester T (2004) The cellular and subcellular localization of neuroglobin and cytoglobin—a clue to their function? IUBMB Life 56(11–12):671–679
96. Lechauve C, Augustin S, Roussel D, Sahel JA, Corral-Debrinski M (2013) Neuroglobin involvement in visual pathways through the optic nerve. Biochim Biophys Acta 1834(9):1772–1778
97. Amunts K, Morosan P, Hilbig H, Zilles K (2012) Auditory system. In: Mai JK, Paxinos G (eds) The human nervous system, 3rd edn. Elsevier, Amsterdam, pp 1270–1300
98. Moore JK (2000) Organization of the human superior olivary complex. Microsc Res Tech 51:403–412